Available online at www.sciencedirect.com
SCIENCE DIRECT®
Progress in Materials Science 49 (2004) 313–345
Progress in Materials Science
www.elsevier.com/locate/pmatsci

Phase diagram calculation: past, present and future

Y. Austin Chang[a,*], Shuanglin Chen[b], Fan Zhang[b], Xinyan Yan[c], Fanyou Xie[b], Rainer Schmid-Fetzer[d], W. Alan Oates[e]

[a]*Department of Materials Science and Engineering, University of Wisconsin, 1509 University Ave., Madison, WI 53706, USA*
[b]*CompuTherm, LLC, 437 S. Yellowstone Dr., Madison, WI 53719, USA*
[c]*Alcoa Laboratories, Aluminum Company of America, Alcoa Center, PA 15069, USA*
[d]*Institute of Metallurgy, University of Clausthal, D-38678 Clausthal-Zellerfeld, Germany*
[e]*Science Research Institute, University of Salford, Salford M5 4WT, UK*

Abstract

The past, present and future of phase diagram calculations for multicomponent alloys are reviewed and assessed. The pioneering studies of Van Laar and Meijering in the first half of the 20th century led to the use of phase equilibrium information as a supplement to single phase thermodynamic property data in these calculations. The phenomenological modeling or the Calphad approach is the primary focus of this review due primarily to its great success in calculating multicomponent phase diagrams for technological applications. In this approach, thermodynamic descriptions of multicomponent alloys are obtained by appropriate extrapolations of descriptions obtained for the lower order systems, viz., the constituent binaries and ternaries. Some shortcomings of the Calphad route to obtaining phase diagrams are pointed out. These include (a) the inability of first generation software to always automatically calculate the stable phase diagram of a system given a thermodynamic description and (b) the use of some inappropriate thermodynamic models, particularly those used for ordered phases. The availability of second generation software eliminates the first shortcoming and a physically more realistic model, the cluster/site approximation, has been formulated which is more suitable for describing the thermodynamics of ordered alloys. The results obtained to-date using the new software and the new model open up new avenues for calculating more reliable multicomponent phase diagrams for technological applications.

* Corresponding author. Tel.: +1-608-262-0389; fax: +1-608-262-0389.
E-mail address: chang@engr.wisc.edu (Y.A. Chang).

0079-6425/03/$ - see front matter © 2003 Elsevier Ltd. All rights reserved.
doi:10.1016/S0079-6425(03)00025-2

Contents

1. Introduction

Phase diagrams are the foundation in performing basic materials research in such fields as solidification, crystal growth, joining, solid-state reaction, phase transformation, oxidation, etc. On the other hand, a phase diagram also serves as a road map for materials design and process optimization since it is the starting point in the manipulation of processing variables to achieve the desired microstructures. Until the last decade of the 20th century, phase diagrams were determined primarily by meticulous and costly experimentation. While this approach has been both feasible and necessary for determining phase equilibria of binaries and those of ternaries over limited compositional regions, it is nearly impossible to obtain phase diagrams of ternary and higher order systems over wide ranges of compositions and temperatures. Yet, most if not all real alloys are multicomponent, often more than ten. One of the real challenges in this field has been and still is to use an alternate approach to obtain multicomponent phase diagrams. Although significant progress has been made in the attempt to calculate alloy energies at 0 K and then phase diagrams by ab initio methods, this approach is unlikely to be successful from a technological viewpoint in the foreseeable future. This is due the difficulties in trying to calculate the high temperature alloy thermodynamic properties with the required accuracy [1] even for binary not mentioning higher order alloys. In this paper, we focus our effort primarily on the phenomenological or Calphad route to calculating phase diagrams for systems of primary interest to materials scientists and engineers. The essence of the Calphad route is to obtain the parameters of thermodynamic

models for the Gibbs energies of the constituent phases in the lower order systems, binaries and ternaries, in terms of known thermodynamic and phase equilibrium data. We can then obtain the Gibbs energies of multicomponent alloy phases from those of the lower order systems via an extrapolation method [2]. These Gibbs energy values enable us to calculate reliable multicomponent phase diagrams in many instances. Experimental work is then only required for confirmatory purposes and not for the determination of the whole diagrams.

Phase diagram calculation was initiated nearly a century ago by Van Laar [3,4]. Using ideal and regular solution models, he calculated a large number of prototype binary phase diagrams with different topological features. Van Laar demonstrated the relationship of the characteristic features of a binary phase diagram in terms of the relative thermodynamic stabilities of the phases involved. Nearly half a century later, Meijering extended the work of Van Laar to higher order systems. Using also the regular solution model, Meijering calculated phase diagrams of mostly prototype ternaries exhibiting different topological features in terms of the thermodynamic stabilities of the phases involved [5–9]. The work of these two researchers has made an important contribution to understanding the phase equilibria of alloys as related to the thermodynamic stabilities of the alloy phases in question.

In the intervening years, alloy thermodynamics researchers began to incorporate phase equilibrium data in a limited manner to assist in the evaluation of the thermodynamic properties of alloys. Monographs by Kubaschewski [10,11], Hultgren [12,13] and Brewer [14] summarize these attempts. Even though these books were published in the period from the early 1960s to the 1980s, these researchers had initiated and adopted this approach in thermodynamic assessment as early as the 1950s. Subsequent to the publication of these monographs, alloy thermodynamics researchers began to calculate phase diagrams of real alloy systems, mostly binaries, first using calculating machines and then computers with software developed by themselves [15–32]. Among all these investigators, Dr. L. Kaufman was the one who used computers to systematically calculate phase diagrams for a large number of real alloy binaries and some ternaries. He used rather simple solution models to describe the alloy phases and was able to calculate phase diagrams of many systems for practical utility. He and his co-worker, Dr. H. Bernstein, summarized many of their published results in a monograph, "*Computer Calculation of Phase Diagrams*" [17].

However, it was not until the middle to late 1980s, when a number of phase diagram calculation software packages became available, that phase diagram calculation of complex binaries and higher order systems became feasible. Such software includes the Lukas program [22], ThermoCalc [33], ChemSage [34], FACT [35], and MTDATA [36]. We will in the present paper refer to these programs as the first generation software for phase diagram calculation. With the development of these software packages, more realistic models were formulated for ordered phases [37–42]. These models were all based on the Bragg–Williams approximation [43–45] and can be shown to be mathematically equivalent under certain conditions [42]. It is worth noting that it is always possible to transform the parameters from a model formalism which possesses more constraints to one with fewer constraints, but not the reverse. For instance, it is possible to transform the model parameters of a

formalism based on the bond energy model to the compound energy formalism but not the reverse [42].

Nevertheless, in view of the need for model compatibility in the development of thermodynamic descriptions for multicomponent alloy systems, most of the software programs have adopted the compound energy formalism [37], originally used in ThermoCalc, for ordered phases. Since the Bragg–Williams model does not take into consideration any short range ordering in the lattice, it is thus not able to describe the order/disorder transition, such as γ'/γ transformation in (Ni, Al) alloys. As a result, prototype coherent phase diagrams, such as the fcc coherent phase diagram in the Ni–Al system, cannot be correctly produced using such a model, the disordered and ordered phases having to be modeled separately to achieve the desired result. Even though this is not so important in understanding the stable phase equilibria, it is critical for studying the kinetics of phase transformation as well as the formation of metastable phases, which often occurs with modern processing tools. We will, in a later section, elaborate on this shortcoming as well as others and offer an alternate approach to resolve this dilemma for cases like γ and γ' in Ni–Al alloys.

It is evident from the above discussion that availability of phase diagram calculation software has been instrumental in advancing progress made in this field. In spite of the tremendous advances made in the last decade, serious shortcomings of the first generation software have become evident [46]. This is due to the fact that the algorithms used in calculating phase diagrams were based on local function minimization routines. Unless reliable starting points are provided, either by some separate algorithm or by the user inputting appropriate starting points, this kind of software can lead to the calculation of a metastable phase diagram for the model parameters used. This occurs when the Gibbs energy of a phase exhibits multiple minima, such as a phase with a miscibility gap or an ordered phase. For the ordered phases, a local minimizer requires good initial values for the sublattice species distributions in order to obtain the stable equilibria. Indeed it is not surprising that some of the published calculated phase diagrams are metastable with respect to the authors' model parameters as reported for the first time by Chen et al. [46]. These problems were revealed by these authors who used a second generation software package, PANDAT, to do the calculations [47]. All these mistakes were made for binaries whose phase diagrams are known. Clearly, this does not place great confidence in using such software for calculations on multicomponent systems where the phase diagram is not previously known. Recognizing the shortcomings of the first generation software, Chen et al. [48,49] began to work on the possibility of the automatic calculation of stable phase diagrams. Their initial ideas have been successfully extended to multicomponent systems in recent years with PANDAT being the product from this effort. PANDAT was developed based on global optimization algorithms and always calculates the stable phase diagrams for a given set of thermodynamic parameters. No initial values are required to be provided. On the other hand, the users can always calculate a metastable phase diagram by removing one or more of the stable phases as they wish! We refer to software like PANDAT as second generation software for calculating phase diagrams. Unless noted otherwise, all calculations presented in this paper have been carried out using PANDAT.

In the present paper, we classify the time frame of Van Laars [3,4] and Meijeiring's pioneering studies [5–9] as "the earlier period", and the phase diagram calculation research subsequent to the their works to the introduction of the first generation software as "the past". The period from the first generation software to the introduction of the second generation software as "the present", and the time subsequent to the introduction of the second generation software as "the future". It is with the availability of the second generation software that we are able to improve the thermodynamic models used for ordered phases in order to minimize the problems enumerated above.

In the following, we will first highlight the great success made in the Calphad route in obtaining multicomponent phase diagrams for research and technological applications in Section 2. Then the shortcomings of the present practice in this otherwise sound approach, partially due to the use of the first generation software and partially due to the Bragg-Williams type of formalism used for ordered phases are presented in Section 3. Next our vision for the future in adopting a more realistic approach in representing the Gibbs energy of alloy phases and an improved model for ordered phases; both of which become possible because of the availability of the second generation software are presented in Section 4. In addition, the use of reliably calculated phase diagram and thermodynamic information for materials research in allied fields such as solidification, solid-state phase transformation and reaction, bulk metallic glasses, oxidation et al., as well as technological applications in materials design and processing simulation is also discussed in Section 4. Finally, the conclusions are given in Section 5.

2. Success achieved using the calphad route to obtain multicomponent phase diagrams

Fig. 1 shows the phenomenological route in calculating phase diagrams of a multicomponent alloy system. In essence, thermodynamic descriptions of the constituent lower order systems, normally binaries and ternaries, are obtained based on experimental and "first principles" total energy information and phase equilibrium data. The term "thermodynamic description" means that a set of thermodynamic models with parameters for phases in a system are obtained so that not only thermodynamic properties of the phases but also phase diagrams of the system can be calculated. However, once descriptions for the lower order systems are known, it is possible in many cases to obtain thermodynamic descriptions of the higher order systems by using an extrapolation method so that phase diagrams of the multicomponent system can be calculated. Although there are a number of such geometrical methods to make these extrapolations [2], the most often used one is that due to Muggianu et al. [50]. It is obvious that the calculated multicomponent phase diagrams must be verified by key experiments, but the amount of experimental efforts involved is insignificant comparing to the traditional approach using exclusively experimental determination. For the rare cases when quaternary phases do exist in systems such as some of the quaternary aluminum alloys [51–53], optimization of model parameters for the quaternary phases in question is necessary. However, the amount of effort involved is minimum normally.

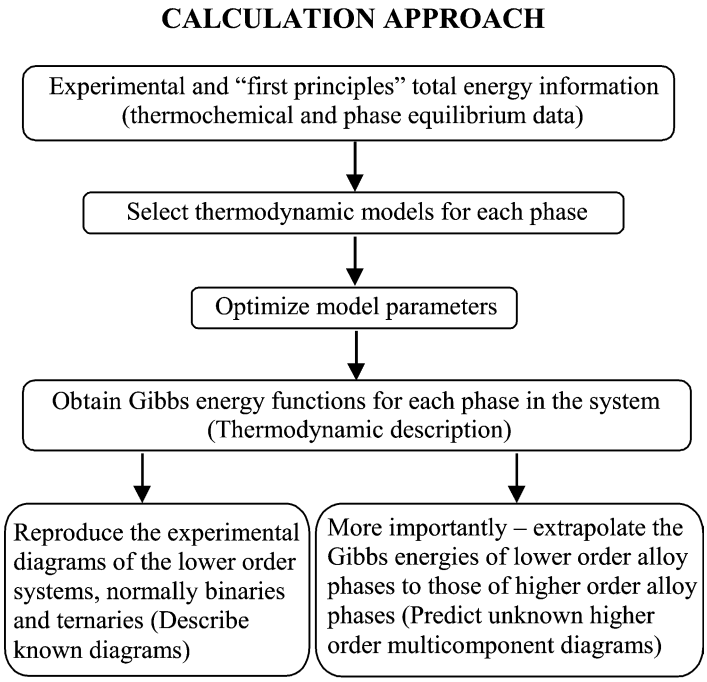

Fig. 1. The Calphad or phenomenological approach used to obtain a thermodynamic description of a multicomponent system.

In the following, we will present three examples to show the successful aspect of Calphad approach, one is for the Ti–Zr–Cu–Ni system and the others are for subsystems of a multicomponent aluminum alloy system [54]. It is worthwhile noting at this point that phase equilibria are governed by the relative Gibbs energies of the phases in question. It is not uncommon that changes even as small as 50 J $(mol)^{-1}$ (we will always use "mol" to mean one mole of atoms unless indicated otherwise) can make a significant shift in the calculated equilibria. This means that accurate phase equilibrium data are always needed for the lower order systems in order to obtain reliable thermodynamic descriptions. In many cases, neither experimental nor "first principles" calculated energy or enthalpy values are accurate enough to differentiate which of the different possible phase equilibria is the stable one. This means that thermodynamic information combining with phase equilibrium data are needed to obtain a thermodynamic description.

Yan et al. [55] obtained a thermodynamic description for the quaternary Zr–Ti–Cu–Ni system by extrapolation based on the descriptions of the constituent binaries and ternaries. Although there is no direct experimental phase equilibrium data for this quaternary, the calculated compositions of the low-lying liquidus surfaces, which should exhibit tendencies for glass formation, are in accord with the experimental findings of Lin and Johnson [56]. It is well known that the formation of glasses occurs at compositions with deep eutectics. One such classical example is a

soda silicate glass with a composition of 76 mol% SiO_2; and this composition is a eutectic point in the pseudobinary Na_2O–SiO_2 [57]. For a higher order system, potential compositions exhibiting great tendencies for glass formation must correspond to alloy compositions on the low-lying liquidus surfaces. For this quaternary, Yan et al. [55] calculated the temperatures for the five-phase invariant equilibria with one of these phases being liquid. They then calculated the compositions of the liquid at these invariant equilibria. The calculated compositions of these liquids at 18 such invariant equilibria are shown in Fig. 2. Also shown in this figure are the alloy compositions found experimentally by Lin and Johnson for bulk metallic glass formation [56]. Indeed it is surprising that the compositions of the model-calculated liquid alloys at these invariant equilibria fall in the same two compositional regimes found experimentally for glass formation. It is reasonable to conclude that the obtained thermodynamic description for this quaternary is acceptable.

Fig. 3 shows a calculated isopleth in terms of T versus x_{Zn} for six component Al alloys Al-Zn-0.095Fe-1.28Mg-0.091Mn-0.079Si with the compositions given in at%. This calculation was made using a recently developed thermodynamic database for 14 component aluminum alloys [54]. Three key quaternaries in this multicomponent alloy system, Al–Cu–Mg–Zn, Al–Cu–Mg–Si and Al–Fe–Mg–Si, which exhibit new quaternary phases have been thermodynamically modeled [51–53]. Moreover, the validity of this thermodynamic database has been evaluated not only in terms of

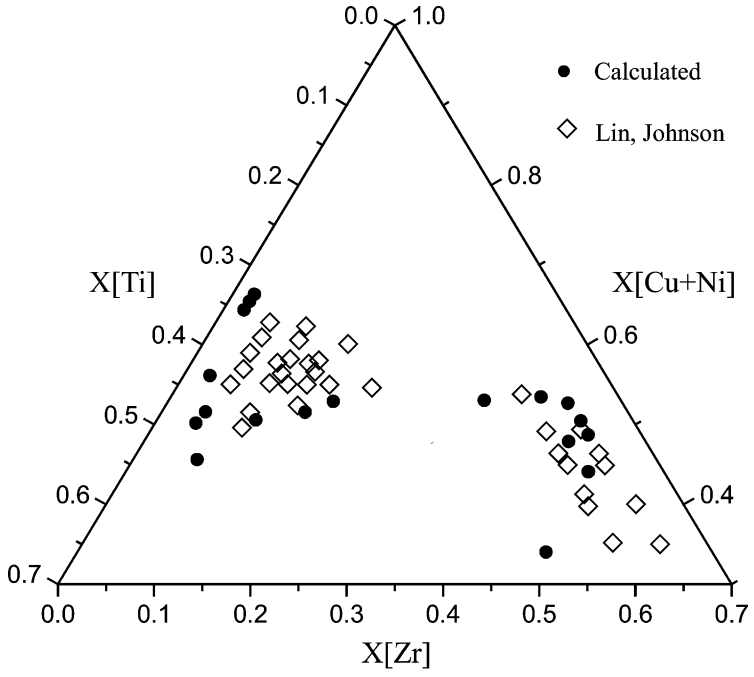

Fig. 2. Comparison of the thermodynamically predicted compositions of quaternary Zr–Ti–Cu–Ni liquid alloys at the five-phase invariant equilibria with those determined experimentally for bulk glass formation by Lin and Johnson [56].

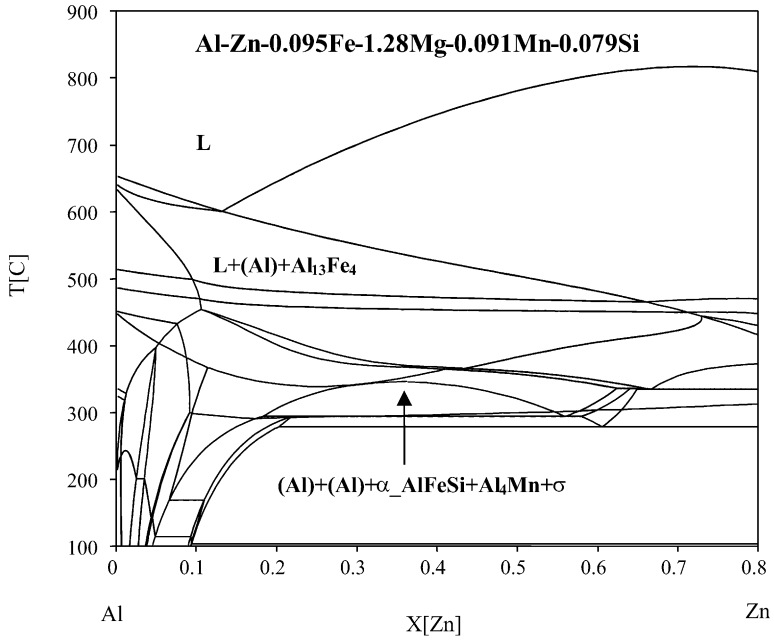

Fig. 3. A calculated isopleth of Al-Zn-0.095Fe-1.28Mg-0.091Mn-0.029Si (in at.% of the component elements).

known phase diagram data but also with results obtained from directional solidification experiments to be presented later in this paper. Since most of the experimental data used to obtain the thermodynamic description are for Al-rich alloys, the reliability of the calculated isopleth shown in Fig. 3 is obviously better with compositions rich in Al. It should be noted that this figure displays a miscibility that is easily overlooked using a first generation software. This is particularly true since it is an isopleth of six component alloys. For such a complex multicomponent system, *it is indeed difficult for a user to realize the existence of a miscibility gap prior to calculating a phase diagram using a first generation software*!

In addition, we present two calculated liquidus projections, one for ternary Al–Cu–Mg and the other for quaternary Al–Cu–Mg–Zn as shown in Figs. 4 and 5 respectively. Representations of the liquidus projection follow the format of Chang and co-workers [58–60] adopting the notations of Rhine [61]. A liquidus projection of Al-rich Al–Cu–Mg alloys is presented in Fig. 4. The traces of the liquidus valley, i.e. the monovariant equilibria, are plotted as well as isothermal contours at 20 °C interval. The primary phases of crystallization are given on each side of the traces of these valleys. As shown in this figure, there are several invariant four-phase equilibria of type I and type II denoted as I_1, I_2 and II_1 etc. and two saddle points denoted as s_1 and s_2. A similar liquidus projection is presented in Fig. 5(a) for the Al-rich region of the quaternary Al–Cu–Mg–Zn system and a reaction scheme is presented as Fig. 5(b). Whilst it is straightforward to visualize the liquidus projection of a ternary such as that shown in Fig. 4, it is more difficult to visualize that for a quaternary as shown in

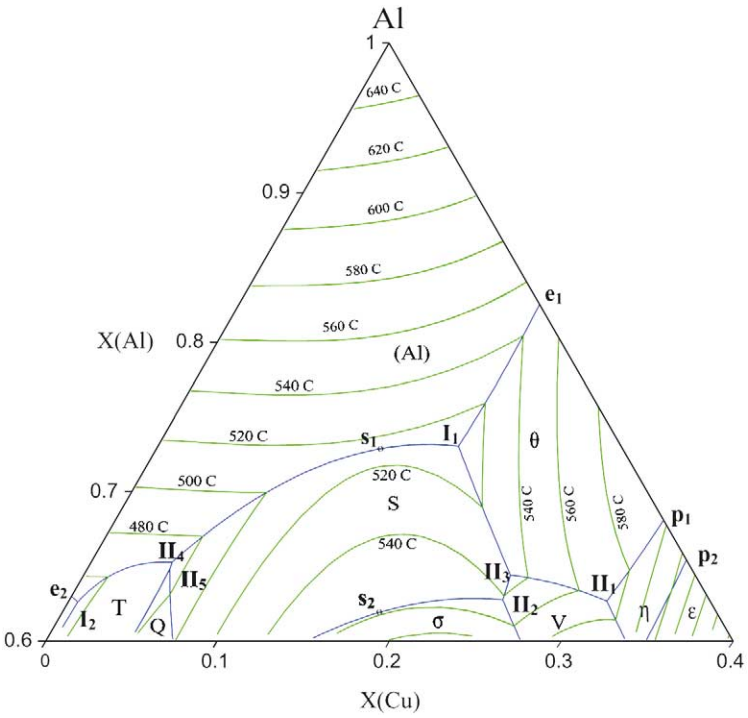

Fig. 4. A calculated liquidus projection of Al-rich corner of the Al–Cu–Mg system.

Fig. 5(a). However, the reaction sequence in Fig. 5(b) helps us to comprehend the liquidus projection shown in Fig. 5(a). In order to differentiate the difference between the traces of the three-phase monovariant equilibria in ternaries from the four-phase monovariant equilibria in the quaternary Al–Cu–Mg–Zn system, different colors are used, blue for the ternary and red for the quaternary monovariant equilibria. In contrast to the four-phase invariant equilibria in ternaries, the five-phase invariant equilibria in the quaternary are denoted as $II_1(q)$ and the saddle point as $s_1(q)$ respectively. As shown in Fig. 5(a), the ternary eutectic I_1, i.e. $L+(Al)+\theta+S$, extends into the quaternary space, intersecting three other four-phase equilibria, i.e. $L+S+\sigma+\theta$, $L+(Al)+S+\sigma$, and $L+(Al)+\sigma+\theta$, to form a type II five-phase invariant equilibrium, $L+S \overset{467.1C}{\rightarrow} (Al)+\sigma+\theta$. The three four-phase equilibria above the five-phase invariant reaction are shown in Fig. 5(a) with arrows pointing downward in temperature toward the five-phase invariant equilibrium while the 4th four-phase equilibrium is shown with an arrow pointing downward away from the invariant equilibrium. The other four-phase equilibrium below the invariant reaction is $(Al)+\theta+S+\sigma$ with all of the phases being solid. One may raise the question where the four-phase equilibrium, $L+S+\sigma+\theta$ originates. The reaction sequence shown in Fig. 5b provides the answer; this four-phase equilibrium comes from II_1, II_2 and II_3 in Al–Cu–Mg (see Fig. 4) through another five-phase invariant reaction $III_1(q)$. If all the traces for these liquidus valleys are plotted in

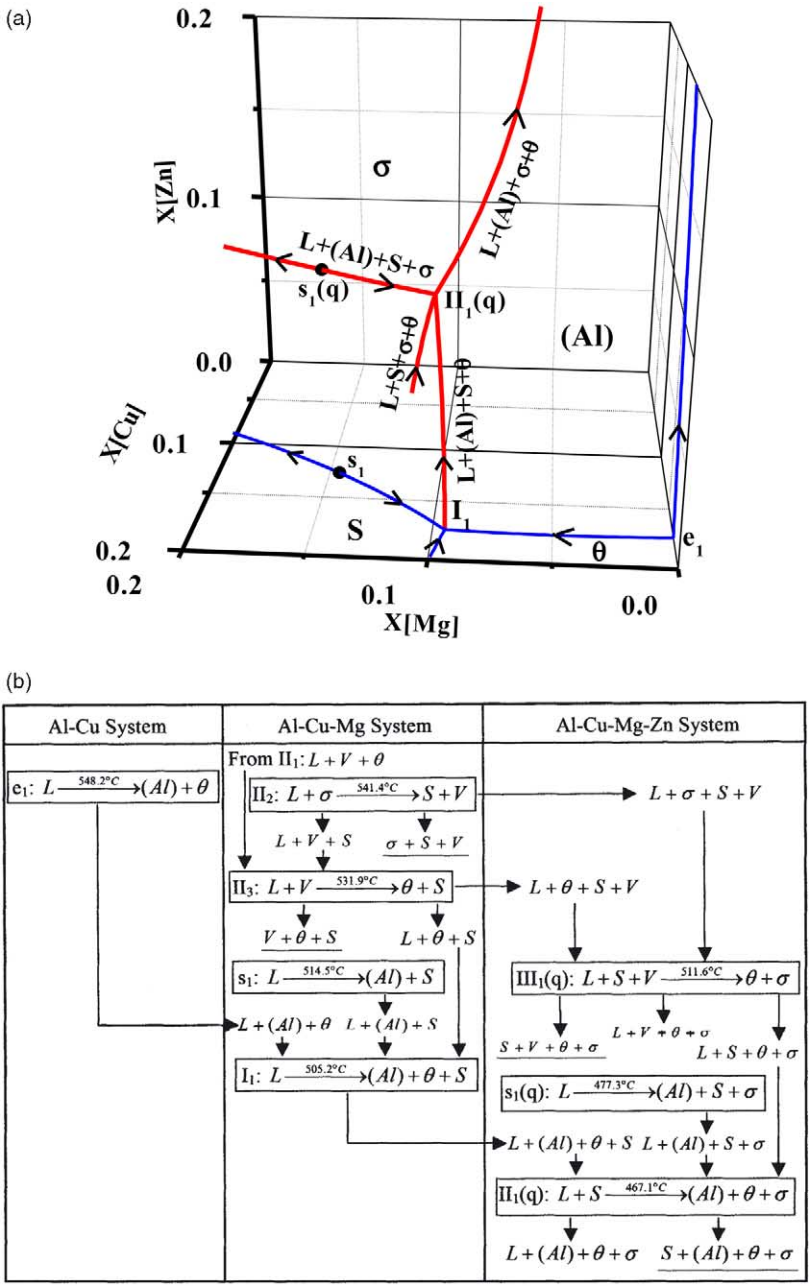

Fig. 5. (a) A calculated liquidus projection of Al-rich corner of the quaternary Al–Cu–Mg–Zn system. The blues lines are the traces of the ternary liquidus valleys (viz. the liquid in equilibrium with two solid phases) and the red lines are those of the quaternary liquidus valleys (viz. the liquid in equilibrium with three solid phases). The four-phase equilibrium, $L+S+\sigma+\theta$, originates from ternary Al–Cu–Mg as shown in Fig. 5(b). (b) Reaction scheme for the Al-rich quaternary Al–Cu–Mg–Zn system.

Fig. 5(a), this figure would become too busy for visualization. This liquidus projection presented in Fig. 5(a) will be used as a reference for a calculated solidification path of a quaternary Al-rich (Al,Cu,Mg,Zn) alloy to be presented later in this paper as Fig. 20.

3. Some shortcomings of the Calphad route in calculating phase diagrams

In spite of the great strides made in the Calphad route to obtaining phase diagrams as noted in the last section, there remain obvious shortcomings. Some of these shortcomings are (1) the inability of the first generation software to reliably calculate the stable phase diagram of an alloy system and (2) the inadequacy of the thermodynamic models currently used by the Calphad community for ordered phases. In the following, we will first present several examples to illustrate these shortcomings and then present an alternative for improving the methodology currently used in the Calphad approach.

3.1. Shortcoming of the first generation software

Since the first generation software uses local optimization algorithms, there is no guarantee that the stable phase diagram will be calculated given a thermodynamic description, or a set of thermodynamic model with parameters, unless the user always inputs the appropriate initial values. However, some of the software mentioned earlier, such as ChemSage and MTDATA, appear to have developed algorithms which eliminate the need for user supplied initial values. As an example shown in Fig. 6, the Gibbs energy for one of the two phases, viz. β, has a double minima because this phase separates into two phases with the same crystal structure but different compositions at low temperatures. In other words, a miscibility gap forms. These two phases are designated as β' and β'' as shown in Fig. 6. This means that three possible phase equilibria may exist between them, i.e. $\beta' + \beta''$, $\beta' + \alpha$, and $\beta'' + \alpha$. But only one of them corresponds to the stable equilibrium, viz. $\beta'' + \alpha$. The situation is more complex when a Bragg–Williams type of sublattice model is used for an ordered phase. When this is the case, the first generation software would depend on the user providing appropriate sublattice species concentrations to calculate the stable phase equilibria, otherwise a metastable phase diagram may be calculated. The user is normally satisfied when the calculated diagram agrees with the experimental one and does not give any consideration to the possibility that the calculated phase diagram may be a metastable one or may only be part of the whole diagram with respect to the model parameters used. These problems were not revealed until the second generation software such as WinPhad [62] and PANDAT [47] became available. These software programs automatically calculate the stable phase diagram as the default without the necessity of the user providing any initial values. Chen et al. [46] have presented numerous cases that the stable phase diagrams calculated by WinPhad and PANDAT using the authors' published parameters do not correspond to the diagrams calculated by the authors. Had they

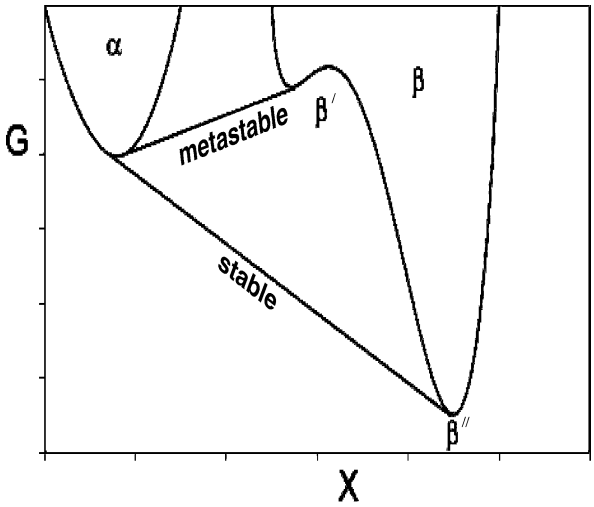

Fig. 6. Gibbs energies of α and β as a function of composition at constant T and p with β exhibiting phase separation. There are three possible phase equilibria but only one of them corresponds to the stable one, viz. $\alpha + \beta''$.

selected initial values at different temperatures and compositions, they might have found that their calculated equilibria are indeed metastable not the stable ones. They would then have to go back to re-optimize their model parameters for the system they are trying to assess. It thus seems a blessing that the second generation software is now available and always gives the stable phase diagrams for a given a set of thermodynamic parameters. Indeed when developing thermodynamic databases for several alloy systems such as that for Ni-base superalloys using PANDAT and WinPhad, Zhang [63] found many published binary descriptions which do not yield phase diagrams in agreement with the experimental one. She then had to re-optimize the model parameters for the binaries so that reliable databases for the multicomponent system could be established. Since binaries are the foundation of any multicomponent system, any incorrect or inappropriate binary model parameters may cause serious problems to the multicomponent database.

In general, three types of unintended phase equilibria are obtained using published binary thermodynamic descriptions. They are inverted miscibility gaps in the liquid phase at high temperatures, the unwanted existence of ordered phases according to the model parameters which were missed in the original calculations, and phases which are stable at low temperatures again becoming stable at higher temperatures. The inverted miscibility gaps appear in the liquid phase with a critical point at low temperature and undergoes phase separation at higher temperatures is shown in Fig. 7 for Sn–Zr [64]. This is due to the unusually large negative entropy used to describe the liquid phase, which makes the Gibbs energy values more positive as the temperature increases. Had these experienced assessors had a second generation software at their disposal, they would have discovered this problem immediately and fixed it accordingly. Two other examples are given in Figs. 8 and 9. In Fig. 8, a low-temperature

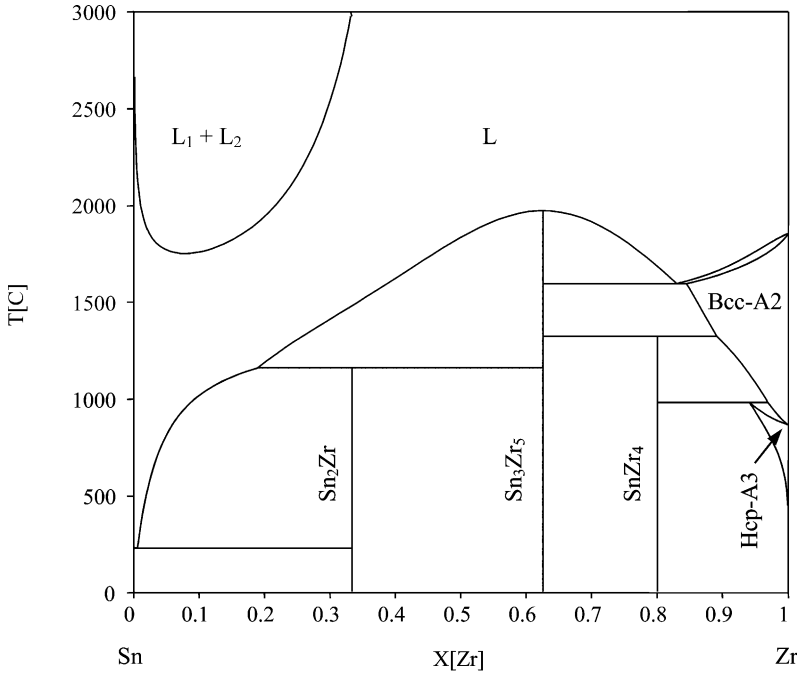

Fig. 7. A Sn–Zr phase diagram calculated using a thermodynamic description published in the literature [64]. The existence of an inverse miscibility in the liquid was overlooked by the authors who used a first generation phase diagram calculation software.

phase Ni_3Ti becomes stable again at higher temperatures, and in Fig. 9, bcc-B2 phase appears at approximately 50–60 at.% Nb at low temperatures where it is not supposed to be stable at all.

3.2. Some shortcomings of the solution models used for ordered phases

Although several solution formalisms have been used for ordered phases in Calphad calculations, all of them are based on the Bragg–Williams approximation. The most commonly used formalism is the compound energy formalism (CEF) developed by Hillert and co-workers [37,65–67,38]. Since this formalism was adopted in ThermCalc [33], it soon became the de facto formalism for describing the thermodynamics of the ordered phase because of the need for model compatibility when extending thermodynamic descriptions from lower order to higher order multicomponent systems. The Gibbs energy of this class of phases at constant p and T is given below for a two-sublattice model as,

$$G^{ord} = \sum y_p^{(i)} y_q^{(j)} G_{(p:q)} + RT \sum f_i y_p^{(i)} \ln y_p^{(i)} + \sum y_p^{(i)} y_q^{(i)} y_r^{(j)} \sum_k \mathrm{L}_{(p,q:r)}^{(k)} \times \left(y_p^{(i)} - y_q^{(i)} \right)^k \quad (1)$$

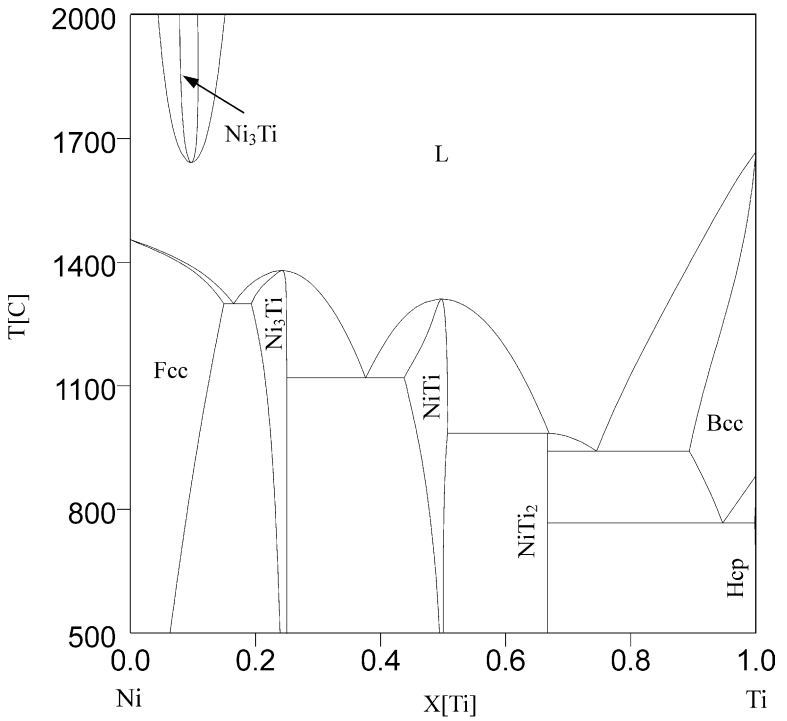

Fig. 8. A Ni–Ti phase diagram calculated from a published thermodynamic description [104]. The reappearance of Ni_3Ti at higher temperatures in the liquid was overlooked by the authors who used a first generation phase diagram calculation software.

where G^{ord} is the Gibbs energy expressed as a function of the sublattice species concentrations. The first term on the RHS of the above equation is the reference state Gibbs energy, the second term is the ideal entropy of mixing on the sublattices and the last term is the excess term, accounting for deviations from ideal behavior. More complicated excess terms have been used sometimes. The quantities R and T are the gas constant and absolute temperature, the y's are the mole fractions of species on a specific sublattice, f_i is fraction of a specific sublattice within the crystal, and $L_{(p,q:r)}$'s are model parameters. The superscripts (i), (j) specify the sublattice in question and the subscripts p and q the species on the sublattice. It is important to point out that each term in Eq. (1) is a function of the sublattice species concentration, which means the Gibbs energy of the ordered phase is completely configurational dependent. We believe that some of the difficulties in describing the thermodynamics of the ordered phases in current practice, to be pointed out later, is due to this formulation to account for the thermodynamic behavior of ordered phases. Too many parameters are needed to describe the experimental data within the compositional and temperature regimes where the phase equilibria are stable. Further, when making extrapolations of the Gibbs energies to metastable regions, unrealistic results are often obtained.

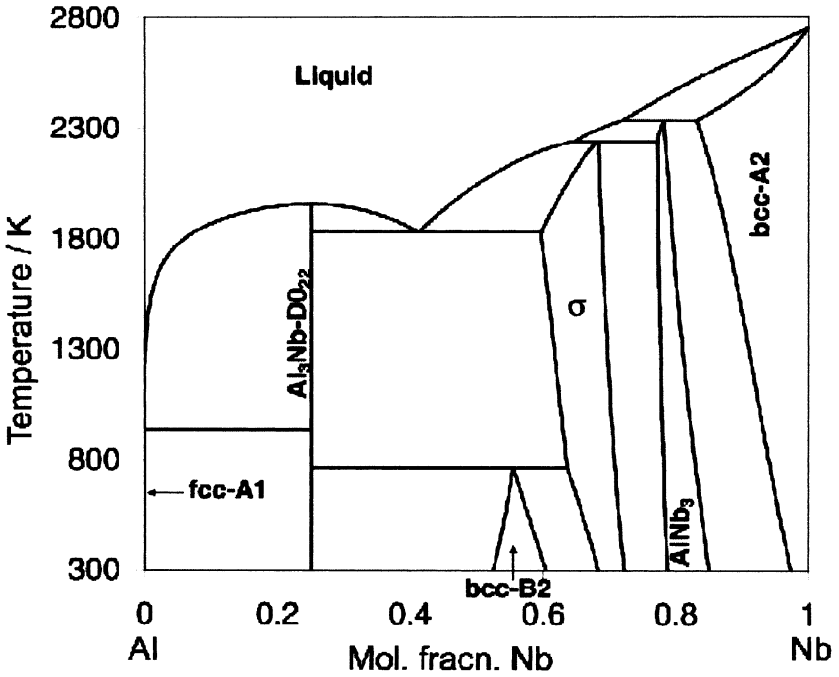

Fig. 9. An Al–Nb phase diagram calculated from a published thermodynamic description [64]. The appearance of a B2 phase over the composition range of about 50–60 at.% Nb was overlooked by the authors who used a first generation phase diagram calculation software.

We now arbitrarily divide ordered phases in two classes. This first one is typified by the prototype Au–Cu and Cd–Mg alloys with ordered phases formed at 25, 50 and 75 at% of the second component. All of these ordered phases transform to their respective disordered states with increasing temperatures. The second one corresponds to intermetallic compounds exhibiting rather narrow ranges of homogeneity and normally do not undergo disordering in real alloys. Familiar examples are the sigma and Laves phases. We will present examples to show that improvement can be made in the approach used currently to describe such phases.

A thermodynamic description was published to describe the Cr–Ta binary using Eq. (1) for the C15 (LT) and C14 (HT) Laves phases [68]. The symbols LT and HT denote the high-temperature and low temperature forms of the Laves phases respectively. They are the only intermetallic phases in this binary. A calculated stable phase diagram of Cr–Ta using their thermodynamic description is presented in Fig. 10. This calculated diagram is in agreement with the experimentally determined one. However, this does not automatically mean that the description is a reliable one. Being able to describe the lower order systems is not the purpose of Calphad approach. We are also interested in extrapolating the Gibbs energies of phases in the lower order systems to those in higher order systems. It is likely that these extrapolations will often lead to compositions beyond the stability ranges of phases in the lower order systems. A simple way to test the reliability of the Gibbs

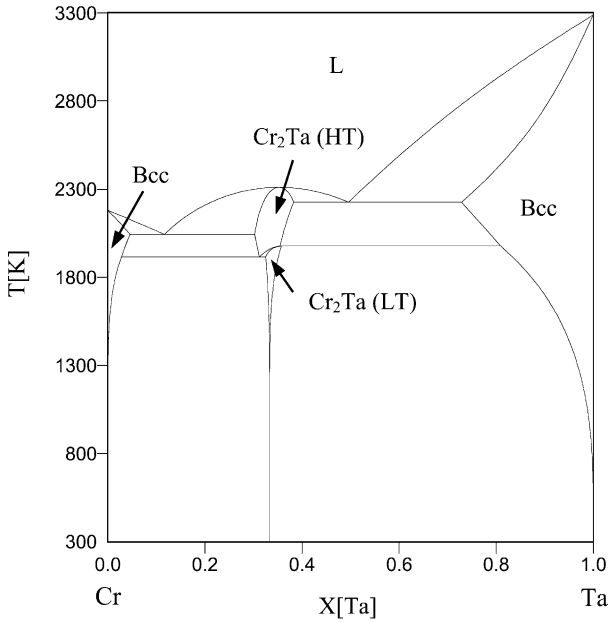

Fig. 10. A Cr–Ta phase diagram calculated using the thermodynamic description of Dupin and Ansara [68].

energies obtained for the ordered phases in the binary system is to suspend one or more phases and calculate a metastable phase diagram. This exercise allows us to extrapolate the Gibbs energies of phases to temperatures and compositions where they are normally unstable. For the Cr–Ta case, we can, for example, suspend the liquid phase and calculate a metastable phase diagram of Cr–Ta with only the solid phases. If the thermodynamic models are reasonable, we would expect that the Laves phase transforms to disordered bcc phase with increasing temperature. Such a calculated diagram is presented in Fig. 11 [69]. As shown in this diagram, not only the C15 phase (LT) becomes stable again at high temperatures, the C15 and bcc two-phase field extend to rather high temperatures. Clearly there is a need to improve the thermodynamic description of these phases. It is noteworthy to point out that one can use first-generation software to calculate the phase diagram shown in Fig. 11 once the users know the high-temperature phase equilibria shown in this figure by supplying the appropriate initial values. However, Fig. 11 was automatically calculated by PANDAT without an input by the users.

In view of their technological importance, the Ni–Al and Ti–Al binaries have received much attention in the last two decades in the materials community. Numerous thermodynamic descriptions have appeared in the literature for Ti-Al [30,64,70] and Ni–Al [71–73]. For these two binaries, there exist a number of ordered phases based either on the fcc or the hcp structures. All authors used the Bragg–Williams approximation to model these phases. Fig. 12 shows a calculated fcc-structure based metastable phase diagram of Ti-Al using the description of Zhang et

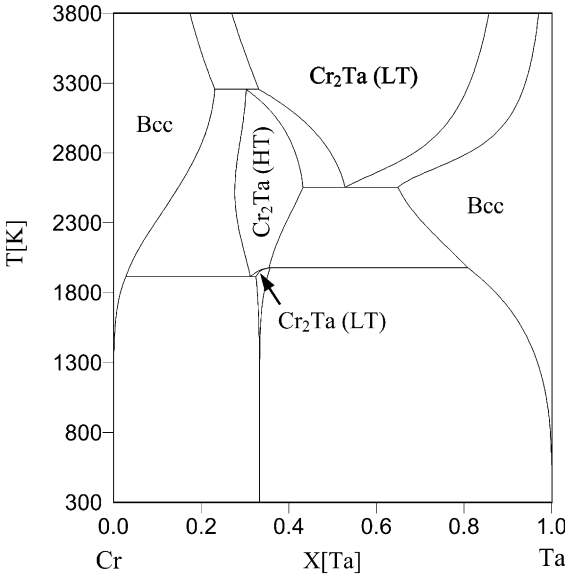

Fig. 11. A metastable solid state Cr–Ta phase diagram calculated using the thermodynamic description of Dupin and Ansara [68]. In other words, the liquid phase is suspended.

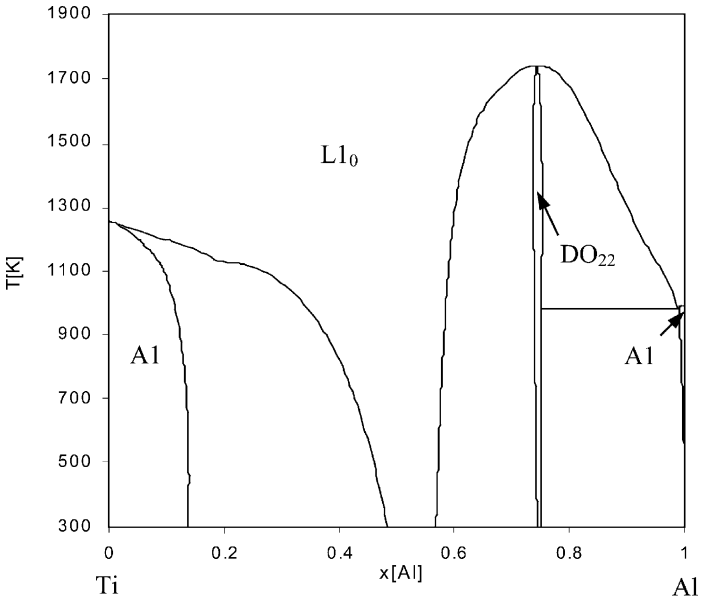

Fig. 12. A metastable fcc-structure based Ti-Al phase diagram calculated using the description of Zhang et al. [70].

al [70]. It is evident from this figure that this calculated metastable diagram is not reasonable. For instance, an ordered phase becomes stable at high temperatures. Fig. 13 shows a calculated fcc-structure based metastable phase diagram for Ni–Al using the description of Huang and Chang [73]. The calculated diagram is likewise physically unreasonable. We have also calculated similar diagrams using other published descriptions of these two systems and found them to be equally unreasonable [74,75]. This is not unexpected since the Bragg–Williams approximation does not take short-range order and other factors into consideration as will be presented later in this paper. Moreover, the large number of added L parameters in order to fit the stable phase boundaries may also be partially responsible. In the next section, we will present an improved approach for calculating phase diagrams in which an attempt is made to minimize these shortcomings and hence may become a promising route for the future.

4. The future in phase diagram calculation

4.1. An improved and realistic methodology for calculating phase diagrams in the realm of the Calphad approach

As shown in Section 2, the Calphad approach is, in our view, the only viable one for calculating multicomponent phase diagrams in the foreseeable future. Availability of

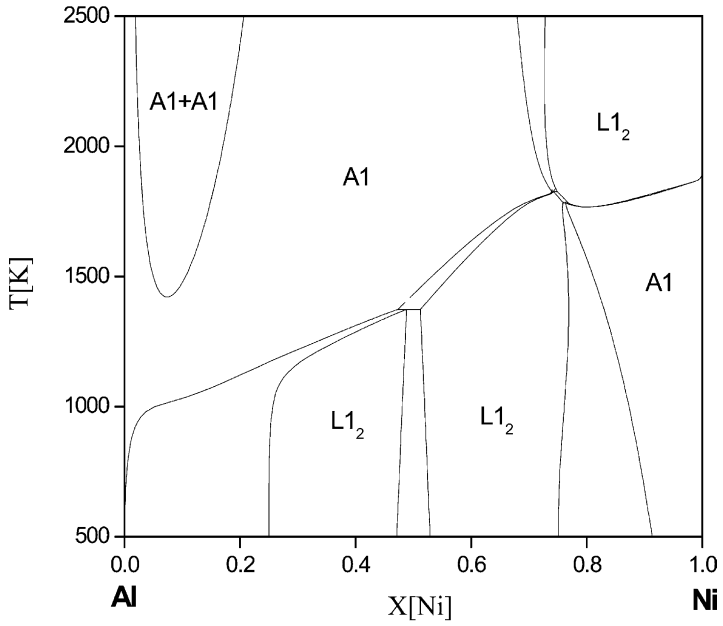

Fig. 13. A metastable fcc-structure based Ni–Al phase diagram calculated using the description of Huang and Chang [73].

second generation software such as PANDAT has made it possible to automatically calculate the stable phase diagram given a thermodynamic description of an alloy system in question without any input information supplied by the user. Metastable phase diagrams can also be easily calculated by suspending some phases in the system at the wish of the user. Examples of such calculations have been presented in Section 3.2. Although continuous improvement is needed for the functionality and efficiency of second generation software, the immediate task for us at the moment is to adopt a new approach to account for the thermodynamic behavior of ordered phases not only for binaries but also for higher order systems.

As presented in Section 3.2, the current practice in accounting for the thermodynamic behavior of ordered phases is based wholly on configuration dependent (CD) contribution as represented by Eq. (1). In other words, the Gibbs energy of the ordered phases is governed entirely by species distributions on the sublattices. This seems unreasonable since there are significant other contributions, such as elastic interactions arising from atomic size mismatch, to the Gibbs energy that depend only on the overall alloy composition and not on the atomic arrangements in that alloy. We refer to this contribution as the configuration independent (CI) term. Accordingly, the Gibbs energy of an ordered intermetallic phase is described as [76]:

$$G = G^{CI}(x_p, T) + G^{CD}(y_p, T) \tag{2}$$

The first term of the RHS of Eq. (2) is the configuration independent term, which depends only on the alloy compositions while the second term configuration dependent which depends on the species distributions on the sublattices. Both configuration dependent and configuration independent terms may be a function of temperature. To retain the necessary simplicity in the Gibbs energy expression for the Calphad approach, we express the configuration independent term using a low order Redlich–Kister polynomial [77]:

$$G^{CI}(x_p, T) = x_p x_q \sum_{\nu=0}^{\nu=2} {}^{(\nu)}\lambda (x_p - x_q)^{\nu} \tag{3}$$

As noted in Section 3.2, we divide ordered phase into two types. For intermetallic phases with small ranges of homogeneity such as the Laves phases, we use the Bragg–Williams approximation to describe the configuration dependent term, i.e., G^{CD} as given by Eq. (1). However, our experience has shown that when the configuration independent term, Eq. (3) is used, the excess configuration dependent Gibbs energy [the last term on the RHS of Eq. (1)] is usually unnecessary. This reduces the total number of model parameters needed to account for the thermodynamics of the phases in question and often makes extrapolation to other compositions more reliable. We have been testing this approach with a number of alloy systems and have so far obtained satisfactory results. Some examples are given below.

Zhang et al. [69] used this approach to describe the Laves phases in Cr–Ta. Eqs. (1)–(3) were used but without the use of any sublattice L parameters in Eq. (1). The

calculated stable phase diagram based on this new description accounts for the experimental data just as well as that published earlier, which was based on using Eq. (1) only [68]. However, the calculated metastable phase diagram in the solid state, i.e., suspending the liquid phase, from the new assessment and shown in Fig. 14 is also quite reasonable. This is evidently clear when comparing the calculated metastable phase diagram using the description of Zhang et al. [69] as shown in Fig. 14 with that in Fig. 11, the latter diagram having been calculated using the previously published description [68]. In their thermodynamic description, Zhang et al. used a subregular solution model, vis. two parameters, to account for the configuration independent term and did not even invoke the excess Gibbs energy for the configuration dependent terms, vis. neglecting the last term of the RHS of Eq. (1). In summary, the total number of parameters used was reduced while a better description was obtained.

For ordered phases which undergo disordering prior to melting such as the prototype Cu–Au and Cd–Mg systems, the Bragg–Willaims approximation is not suitable due to the neglect of short-range ordering in the lattice [78]. Accordingly, we have been using the cluster site approximation (CSA) to account for the configuration dependent term given in Eq. (2). It does consider short-range order and is able to account for order/disorder transitions. The CSA greatly simplifies the calculation effort that is otherwise necessary when directly applying the physically sounder cluster variation method (CVM) [79,80]. It is thus particularly suitable for the calculation of multicomponent phase diagrams.

The cluster site approximation (CSA) was applied to solid alloys by Yang and Li [81–84]. In contrast to the CVM [85], the CSA clusters are energetically *non-interfering*: they are permitted only to share corners. Since there is no cluster overlap, the

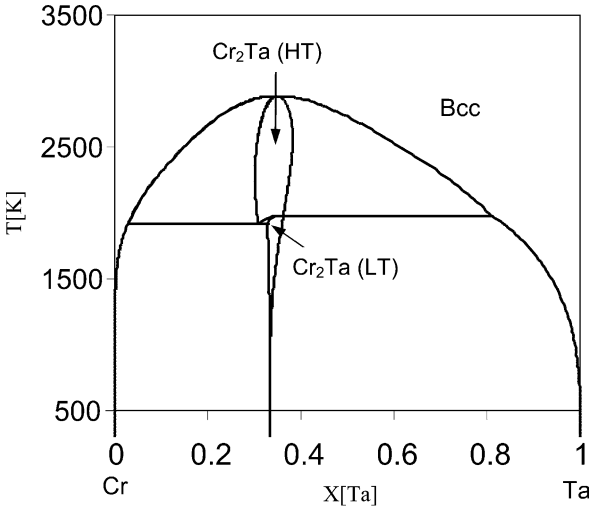

Fig. 14. A metastable solid state Cr–Ta phase diagram calculated using the thermodynamic description of Zhang et al. In other words, the liquid phase is suspended. Compare this calculated diagram with that shown in Fig. 11.

only energy parameters required are the cluster energies themselves, the energies of the sub-clusters do not enter into the energy equation. Moreover, a lack of cluster interference leads to a two-term expression for the entropy of mixing irrespective of the cluster size. Accordingly, the second term on the RHS of Eq. (2) can be written as below,

$$G^{CD} = \gamma RT\left(\sum_{\mathrm{i}=1}^{\mathrm{n}} y_A^{(\mathrm{i})}\mu_A^{(\mathrm{i})} - \ln\varphi\right) - (n\gamma - 1)RT\sum_{q,\mathrm{i}} f_{\mathrm{i}} y_p^{(\mathrm{i})}\ln y_p^{(\mathrm{i})} \tag{4}$$

with the cluster partition coefficient ϕ being obtained from

$$\phi = \left(\sum_{j=1}^{j=2^{\mathrm{n}}} \exp\left[\left(\sum \mu_A^{(\mathrm{i})}\right) - \varepsilon_j\right]\right. \tag{4a}$$

In Eq. (4), the $y_p^{(\mathrm{i})}$'s are the sublattice species concentrations, and the $\mu_A^{(\mathrm{i})}$'s, are related to the species chemical potentials. Since these are uniquely related to the $y_p^{(\mathrm{i})}$'s, only one of them is required as an independent variable. The quantity ϵ_j is the cluster energy of a j-type cluster. The term γ is a geometrical factor originated from the number of non-interfering clusters per site in the original CSA [81–84]. It, in essence, becomes a parameter of the CSA.

Since the clusters in the CSA are energetically non-interfering as shown in Eq. (4), the point probabilities are used as the independent variables, thus retaining the advantage of the Bragg–Williams approximation in terms of computation. On the other hand, it does consider both long and short range order, thus retaining the strength of CVM. The energy parameters are the cluster energies, which can be expressed in terms of a pair interaction energies to further reduce the number of parameters.

It has been found that, when compared with MC calculations, the configurational term for fcc alloys obtained from the CSA slightly underestimates this term whilst that obtained from the CVM overestimates it [80,86,87]. However, the deviations from the CSA results are no worse than those from the CVM. The slight inadequacy of CSA can be overcome by incorporating a geometrical factor γ as given in Eq. (4) [80]. Since, in real alloys, the configurational entropy and Gibbs energy of mixing is often only a small fraction of the total, any small difference between the results obtained from the CSA and CVM is of minor significance. The important thing is that both, unlike the Bragg–Williams models, can give the correct phase diagram topology and that the CSA, unlike the CVM, has the same number of independent variables as in the Bragg–Williams models. These two features make the CSA ideal for multicomponent phase diagram calculations.

In the following, we will give three examples to show that the approach outlined above works quite well and eliminates some of the shortcomings pointed out in Section 3.2. The three examples are (i) the calculated Cu–Au phase diagram is in close agreement with that calculated by the CVM, (ii) the calculated phase diagram of Cd–Mg is in accord with the experimentally determined one, and (iii) the calculated Ni–Al phase diagram is in accord with the experimentally determined one and,

more importantly, the topology of the calculated metastable phase diagram based on the fcc-structure is what one would expect.

Ferreira et al. [88] calculated a Cu–Au phase diagram using the CVM including an elastic energy contribution due to lattice mismatch; the mathematical form of this elastic energy corresponds to the first term of the Redlich–Kister polynomial given in Eq. (3), i.e., ${}^0\lambda$. Using the cluster energy parameters and the values of ${}^0\lambda$ of Ferreira et al. [88], Oates et al. [80] calculated a Cu–Au phase with a value of $\gamma = 1.41$, a geometrical parameter in the CSA model. The calculated phase diagram as shown in Fig. 15 is in good agreement with that calculated by Ferriara et al. [88].

The phase diagram of Cd–Mg is a prototype for the hcp structure like that of Cu–Au for the fcc structure. Using the same approach, Zhang et al. calculated the phase diagram of Cd-Mg [89]. As shown in Fig. 16, the calculated phase diagram is in good agreement with the experimental data of Frantz and Gantois [90]. The five parameters used are $\varepsilon_{Cd_3Mg} = -9.3$, $\varepsilon_{Cd_2Mg2} = -13.7$ and $\varepsilon_{CdMg3} = -9.95$ and ${}^0\lambda = 21.62$ kJ/mol atoms and $\gamma = 1.8$. The model-calculated thermodynamic properties of the alloys are also in accord with experimentally measured values [89]. It is worth pointing out that Asta et al. [91] have calculated the phase diagram of Cd–Mg using the so-called "first principles" method. The calculated phase diagram is topologically similar to that shown in Fig. 16 but the temperatures of the phase transitions are considerably higher. The three cluster energies used by Zhang et al. [89] differ from those used by Asta et al. by 10, 1 and 10% respectively.

The binary Ni–Al is a system of great interest both in terms of science and technology. Fig. 17 shows a calculated phase diagram from the conventional description of Huang and Chan [73]. There exist in this binary the γ-(Ni,Al) phase (fcc) and the ordered γ'-Ni_3Al ($L1_2$) phases. Even though γ' is an ordered form of γ, it does not transform to γ with increasing temperatures under equilibrium condition. Instead γ'

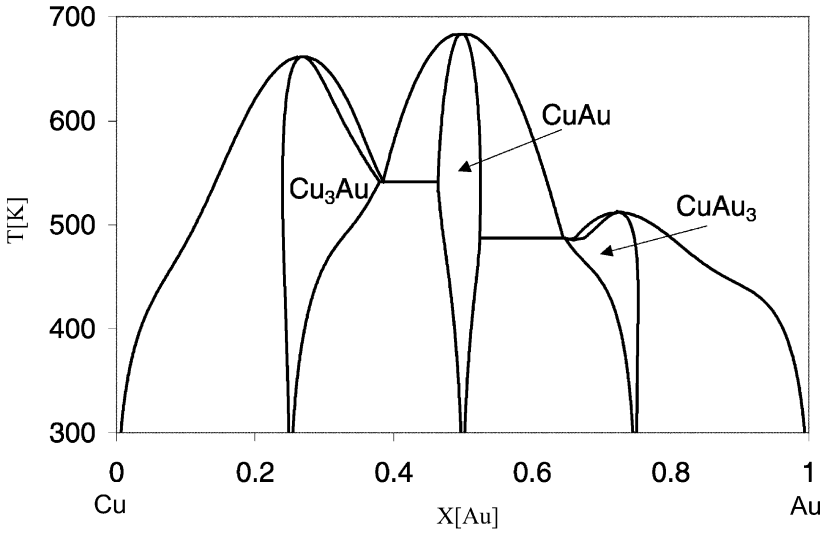

Fig. 15. A Cu–Au phase diagram calculated using the CSA model [80].

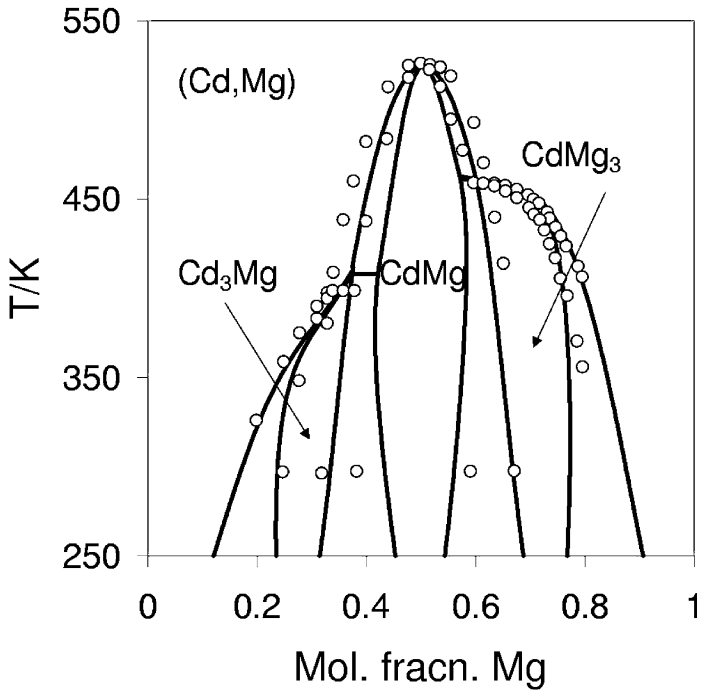

Fig. 16. A Cd–Mg phase diagram calculated using the CSA model [89]. The experimental data were taken from the Frantz and Gantois [90].

melts peritectically to liquid and γ. However, thermodynamically γ' must transform to γ with increasing temperature in the metastable state. On the other hand, the calculated metastable phase diagram of Ni–Al based on the fcc structure according to this description as shown in Fig. 13 does not exhibit the order/disorder transformation. This is due to the fact that a Bragg–Williams type model is used for the γ' phase. More recently, Zhang et al. [75,92] remodeled the Ni–Al system using the CSA to describe the fcc-based alloys. The calculated stable phase diagram of Ni–Al is in as good agreement with the experimental data as that using the description of Huang and Chang [73]. The total number of model parameters used by Zhang et al. is less. Moreover, as shown in Fig. 18, the calculated metastable fcc-structure based phase diagram from the later description is what one would have expected. The γ' phase ($L1_2$) transforms congruently to the fcc γ-phase at 1708 K. The equiatomic $L1_0$ phase exists over a range of homogeneity and also transforms congruently to the fcc γ-phase but a $L1_2$ phase is not stable at 25 at.% Ni. Instead a phase separation of the fcc phase is predicted. It is noteworthy to point out that Sigli and Sanchez [93] and Pasturel et al. [94] have also calculated the Ni–Al phase diagram using the CVM. While the former optimized the cluster energy parameters in terms of experimental data, the latter obtained them from the "first principles" method. The calculated fcc-structure based phase diagram of Ni–Al by Pasturel et al. [94] is

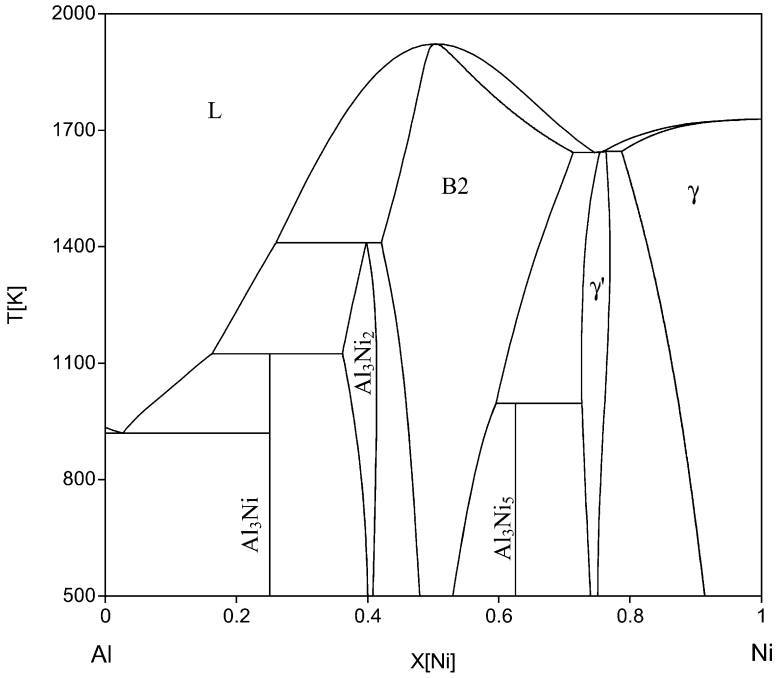

Fig. 17. A Ni–Al phase diagram calculated from the description of Huang and Chang [73].

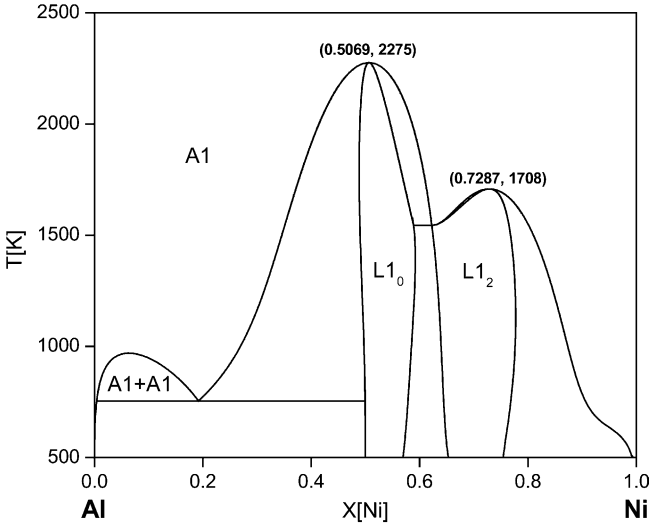

Fig. 18. A fcc-structure based metastable phase diagram of Ni–Al calculated using the thermodynamic description of Zhang et al. [92,75] who used CSA to describe the fcc-structure based phases. Compare this calculated metastable phase diagram with that shown in Fig. 13.

topologically similar to the CSA-calculated diagram shown in Fig. 18, although the calculated transition temperatures are higher than those shown in Fig. 18.

The results presented above for three binary alloys demonstrate beyond any shadow of doubt that the CSA offers a realistic alternative in the calculation of phase diagrams of alloys where ordered phases exist. Based on the results obtained for Ni–Al as noted here and preliminary results for Ni–Cr and Cr–Al, we are currently extending this approach to calculate phase diagrams of ternary Ni–Al–Cr alloys.

4.2. Importance of thermodynamic descriptions in predicting the microstructural evolution during processing of materials: the ultimate goal in predicting the mechanical and functional behavior of materials

Reliable thermodynamic descriptions of materials are the starting point in computing the microstructural evolution of materials during processing via kinetics. Based on these computed microstructures, it becomes possible to predict the mechanical and functional behavior of these processed materials. It is evident from our discussion in this paper that significant progress has been made in the use of the Calphad methodology in developing thermodynamic descriptions of weakly interacting alloys, not only for binaries but also for higher order alloys, i.e. in the absence of a significant degree of ordering. But this is not true for materials with ordered alloys such as the Ni-based alloys involving γ and γ', the fcc phase and its ordered form. We have presented the basic idea in Section 4.1 that the energetic contributions to the Gibbs energy of an alloy consists of two terms, viz., a configuration independent (*depending on the alloy composition*) and a configuration dependent (*depending on the species distributions on the sublattices*) one. The results presented so far show this basic idea is extremely promising. Equally promising is the adoption of the CSA to describe the configurational dependent term for ordered phases. The approach presented in this paper represents the future of the Calphad route to calculate the phase diagrams of multicomponent alloys.

Because computational materials science/engineering is becoming a tool for materials and processing design, it becomes incumbent upon us to try and develop a realistic framework which provides scientifically sound thermodynamic information and which can be integrated readily with kinetic models to predict the microstructure of materials during processing. For the past few years, we have been working on a narrowly focused research project to integrate a 14 component thermodynamic database for aluminum alloys [54] with a modified Scheil model to calculate the microstructures and microsegregation of aluminum-rich alloys under directional solidification condition. The calculated results are compared with results obtained experimentally. We will first give a brief description of the approach used and then the results obtained.

Fig. 19 shows a schematic diagram illustrating an integrated approach to couple phase diagram calculation with kinetics, viz., a solidification model to calculate microsegregation in a solidifying alloy. The inputs to the calculation are the gross composition of the alloy in question and the solidification conditions. In the present case, PanEngine [95,96], the computational engine of PANDAT [47] is used to calculate the

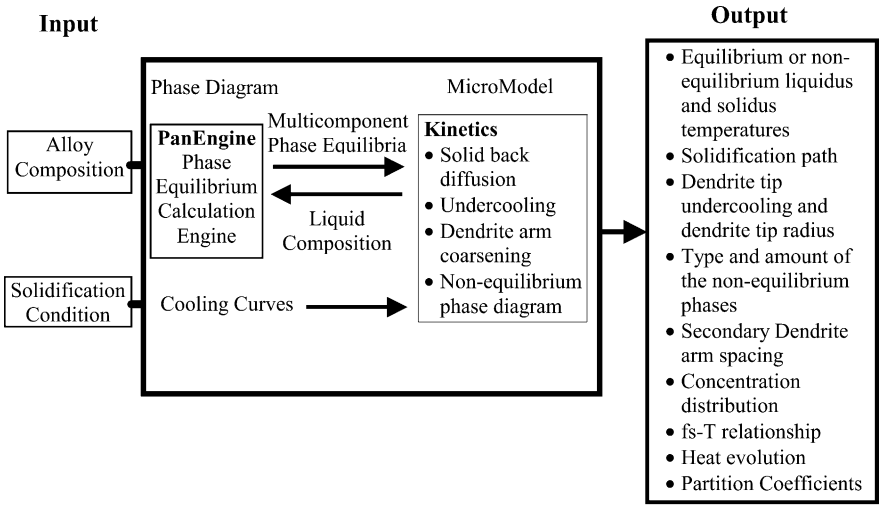

Fig. 19. A schematic diagram illustrating integration of a phase diagram calculation software, PanEngine in this case, with a kinetic model to calculate microsegregation in alloys during solidification.

partition coefficients needed for solidification simulation. Cooling curves obtained from the directional solidification experiments give the solidification condition. The microsegregation model is a one-dimensional modified Scheil model considering solid-state back diffusion, undercooling of the dendrites, coarsening of the secondary dendrites and non-equilibrium phase diagram due to rapid solidification. The outputs of the calculation are listed in Fig. 19, including paths of solidification, dendrite tip undercooling, amounts of the phase formed under non-equilibrium condition, solute re-distribution in the secondary dendrite arm etc. The input data to PanEngine are the Gibbs energy functions from a thermodynamic aluminum database [55] and those to the modified Scheil model include all needed thermophysical properties of alloys such as surface energies, diffusion coefficients etc. We have carried out studies for a number of aluminum alloys from binary Al–Cu, ternary Al–Cu–Mg, quaternary Al–Cu–Mg–Zn to multicomponent commercial aluminum alloys of more than ten components [97–102].

Based on the study of a large number of aluminum alloys, we have come to the conclusion that in order to validate the reliability of a solidification model, it is essential to have experimental data on solute distribution in the secondary arm dendrites. We have found that the measured fractions of solids as a function of temperature are not sufficiently sensitive to validate the solidification models used. On the other hand, the experimentally measured solute distributions within the dendrites are sensitive to test the validity of the model. It is also worth noting that the most sensitive parameter in calculating solute distributions in the secondary dendrite arms is the partition coefficient or the compositions of the solidus. Liang et al. [99] has shown conclusively that even a change of 0.5 at% or less in Al alloys can have a profound influence on the calculated solute distributions. This result indicates that a reliable thermodynamic database is essential in carrying out this kind of study.

In the following, we first report the solidification path obtained for a quaternary aluminum alloy, viz. Al-1.68Cu-1.02Mg-0.42Zn (in at.%) under Scheil condition, and then the microscopic modeling results for an Al 7050 alloy with nine components, i.e. under modified Scheil conditions as shown in Fig. 19. The calculated path of solidification under Scheil condition for this quaternary Al alloy is $L \rightarrow L+(Al) \rightarrow L+(Al)+\theta \rightarrow L+(Al)+\theta+S \rightarrow L+(Al)+\theta+S+\sigma$ as summarized in Table 1 and presented graphically on the liquidus projection of Al–Cu–Mg–Zn as shown in Fig. 20. (The liquidus projection shown in this figure is the same as that in Fig. 5). As can be seen from this figure, the first phase of solidification is (Al), then θ, next S, and lastly σ at the five-phase invariant reaction, $II_1(q)$. Solidification after this five-phase equilibrium continues to even lower temperatures.

Table 1
Reactions during Solidification for the quaternary Al-1.68Cu-1.02Mg-0.42Zn (in at.%) alloy studied (under Scheil condition)

Reaction #	Reactions	Temperature (°C)
1	Al dendrites	644.2
2	Liq. $\rightarrow \alpha+\theta$	510.2
3	Liq. $\rightarrow \alpha+\theta+S$	492.1
4	Liq. $+S \rightarrow \alpha+\theta+\sigma$	467.1

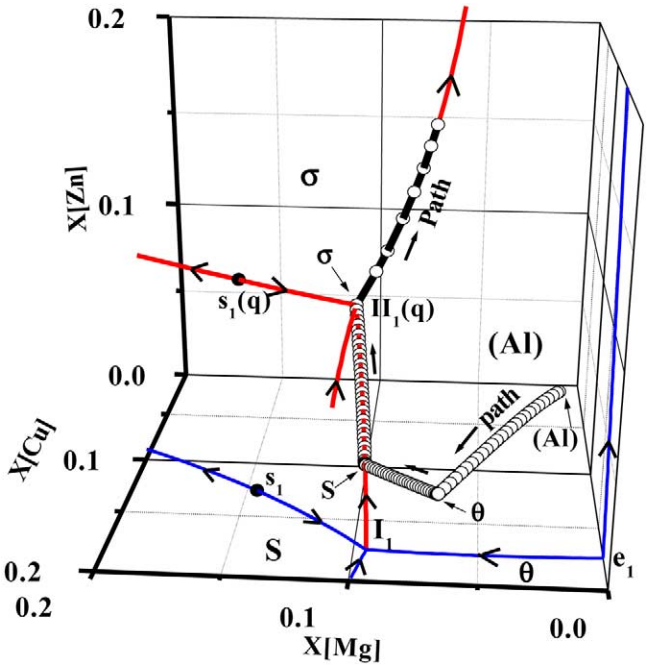

Fig. 20. Graphical representation of a calculated solidification path of a quaternary Al-1.68Cu-1.02Mg-0.42Zn alloy (in at.%) under the Scheil condition. The liquidus projection shown in this figure is the same as that in Fig. 5(a).

The microsegregation results for the multicomponent aluminum 7050 alloy were calculated using the modified Scheil model including the effects of back diffusion in the solid, dendrite arm coarsening and undercooling [103]. The calculated fractions of the solids formed and the secondary arm spacings for this alloy and the solidification conditions are given in Table 2. As can be seen from this table, the calculated results are in good agreement with the experimental measurements. Fig. 21 (a),(b)

Table 2
Comparison of experimental and calculated phase fractions and dendrite arm spacings

Cooling rate (K/s)	Amount of Al Phase, vol.%					λ_2, μm	
	Area Scan	Image analysis	Modified Scheil	Scheil	Lever rule	Image analysis	Modified Scheil
0.45	92.5	94.4	94.8	89.0	98.3	56	55.2

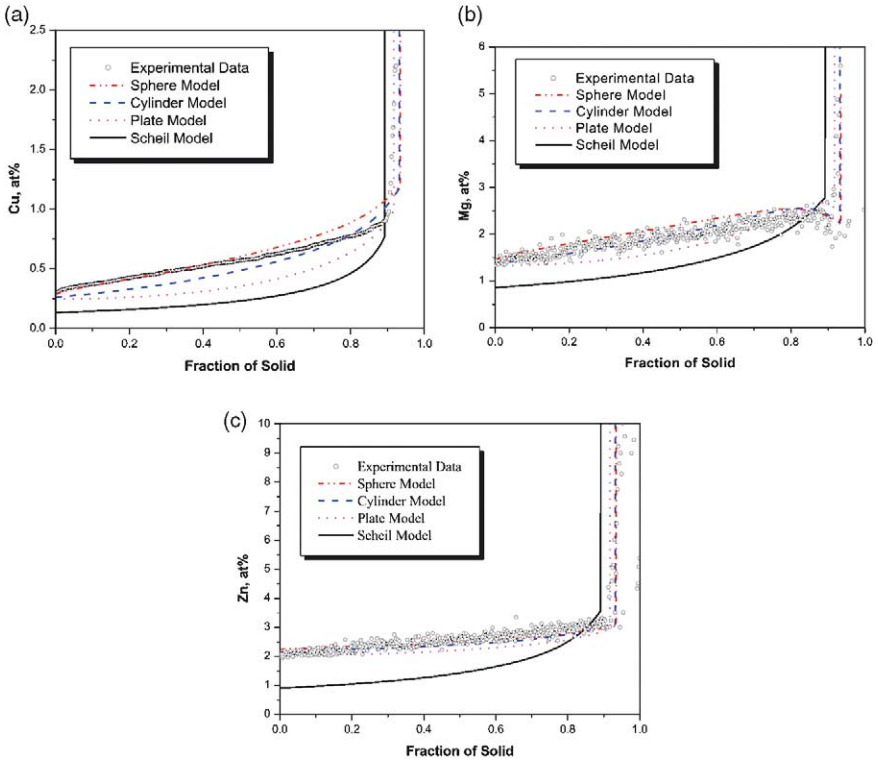

Fig. 21. Comparisons of calculated concentration distributions of solutes within the dendrites of a directionally solidified 7050 Al alloy, Al-1.17Cu-2.78Mg-2.86Zn-0.016Cr-0.046Fe-0.026Mn-0.005Ni-0.061Si-0.011Ti-0.031Zr (in at.%), using a modified Scheil model with experimentally measured values [103] at a cooling rate of 0.45 C/sec. Three geometrical models were used to approximate the shapes of the dendrites, i.e. plate, cylinder and sphere. (a) Cu, (b) Mg and (c) Zn.

and (c) shows the calculated solute distributions for the major alloying elements. These calculated results are in good agreement with experimental data obtained from directional solidification. The solute distributions calculated from the Scheil condition deviate from the experimentally measured values. Detailed descriptions of the solidification modeling, the experimental method used, and the results obtained are given elsewhere [97,98,103].

These examples show that a phase diagram calculation software such as PanEngine together with a reliable thermodynamic database can be integrated with kinetics modeling in a seamless manner to predict microstructural evolution of multicomponent alloys during processing and ultimately their mechanical behavior.

5. Conclusion

The past, present and future in phase diagram calculation for multicomponent alloys has been reviewed and assessed, focusing primarily on the phenomenological modeling or the Calphad approach. In this approach, thermodynamic descriptions of multicomponent alloys are obtained based on descriptions of the lower order systems, viz., normally the constituent binaries and ternaries. The lower order thermodynamic descriptions are obtained primarily in terms of experimentally determined thermodynamic properties and phase equilibrium data. Although ''first principles'' calculated 0 K energetics of alloys are being used in the modeling of binaries, this approach is not yet able to calculate phase diagrams for technological applications. Following the pioneering studies of Van Laar and Meijering in the first half of the 20th century, phase equilibrium information was used to assist in the assessment of measured thermodynamic data (from the late 1950s to the 1980s). This period is considered ''the past'', the advent of the first generation software to the introduction of the second generation software in the late 1990s as ''the present'', and the time subsequent to the second generation software as ''the future''.

Highlighting the great success of the Calphad route in obtaining multicomponent phase diagrams for technological applications, notable shortcomings have been noted. One of these shortcomings is the inability of the first generation software to automatically calculate the stable phase diagram of an alloy system in question when a thermodynamic description is given. The other shortcoming has been the formalism used to describe the Gibbs energy of alloy phases and, particularly, the use of Bragg–Williams models to represent the Gibbs energy of ordered phases. Examples have been presented which highlight these shortcomings and the second generation software such as PANDAT has resolved this shortcoming. In addition, an alternate and realistic methodology was formulated to account for the Gibbs energies of alloy phases in the realm of a Calphad approach to calculate phase diagrams. The results obtained so far have demonstrated the great utility of the newly formulated methodology in calculating multicomponent phase diagrams.

Acknowledgements

One of the authors YAC wishes to acknowledge the financial support of NSF, INCRA, DARPA, NASA, AF, DOE, ALCOA and Wisconsin Distinguished Professorship for materials research conducted at the University of Wisconsin in thermodynamics and kinetics and the application of thermodynamics and kinetics to extraction/refining, mechanical-driven, and electronic-driven materials over the years and SLC, FZ, FYX and YAC the financial support of the Air Force Research Laboratory, Wright–Patterson AFB, OH through SBIR projects for work done at CompuTherm, LLC, Madison, WI.

References

[1] Oates WA, Zhang F, Chen S-L, Chang YA. Future directions in the calculations of multi-component real-alloy phase diagrams. Acta Mater. 2003, to be submitted.
[2] Chou K-C, Chang YA. A study of ternary geometrical models. Ber Bunsenges Phys Chem 1989;93:735.
[3] Van Laar JJ. Z Phys Chem 1908;63:216.
[4] Van Laar JJ. Z Phys Chem 1908;64:257.
[5] Meijering JL. Segregation in regular ternary solutions, Part I. Philips Res Rep 1950;5:333.
[6] Meijering JL. Segregation in regular ternary solutions, Part II. Philips Res Rep 1951;6:183.
[7] Meijering JL, Hardy HK. Closed miscibility in ternary and quaternary regular alloy solutions. Acta Metall 1956;4:249.
[8] Meijering JL. Calculation of the nickel-chromium-copper phase diagram from binary data. Acta Metall 1957;5:257.
[9] Meijering, J.L. Thermodynamical calculation of phase diagrams. In: Physical chemistry of metallic solutions and intermetallic compounds. New York: Chemical Publishing Company, Inc.; 1960, 124–42.
[10] Kubaschewski O, Alcock CB. Metallurgical Thermodynamic Chemistry. 4th ed. Oxford, UK: Pergamon Press; 1967.
[11] Kubaschewski O, Alcock CB. Metallurgical thermodynamic chemistry. 5th ed. Oxford, UK: Pergamon Press; 1979.
[12] Hultgren R, Orr R, Anderson P, Kelley KK. Selected Values of the Thermodynamic Properties of Binary Alloys. New York: John Wiley and Sons; 1963.
[13] Hultgren R, Desai PD, Hawkins DT, Glesier M, Kelley KK. Selected Values of the Thermodynamic Properties of Binary Alloys. Metals Park, OH: American Society for Metals; 1973.
[14] Brewer L, Lamoreaux RH. Thermochemical properties. In: Molybdenum: physico-chemical properties of its compounds and alloys, International Atomic Energy Agency, Vienna, 1908, 11-191 and Brewer L, Lamoreaux RH. Phase diagrams. In: Molybdenum: physico-chemical properties of its compounds and alloys, Vienna: International Atomic Energy Agency; 1908;195-356.
[15] Rudy E. Z Metallk 1963;54:112–22.
[16] Rudy E. Z Metallk 1963;54:213–23.
[17] Kaufman L, Bernstein H. Computer calculation of phase diagrams. New York: Academic Press; 1970.
[18] Pelton AD, Schmalzried H. Metall Trans 1973;4:1395–404.
[19] Spencer PC, Barin I. Mater in Engin Applications 1979;1:167–79.
[20] Sharma RC, Chang YA. Thermodynamics and phase relationships of transition metal sulfur systems III. Thermodynamic properties of the Fe-S liquid and the calculation of the Fe-S phase diagram. Met Trans 1979;10B:118.
[21] Hillert M. Physica B 1981;103:31.

[22] Lukas HL, Weiss J, Henig E-Th. CALPHAD 1982;6:229.
[23] Gabriel A, Gustafson P, Ansara I. CALPHAD 1987;11:203.
[24] Schmid R. A thermodynamic analysis of the Cu-O system with an associated solution model. Metall Trans B 1983;14B:473.
[25] Chuang Y-Y, Hsieh K-C, Chang YA. Thermodynamics and phase relationships of transition metal sulfur systems V. A re-evaluation of the Fe-S binary system. Met Trans 1985;16B:277.
[26] Chuang YY, Chang YA, Schmid R, Lin J-C. Magnetic contributions to the thermodynamic functions of alloys and the phase equilibria of the Fe-Ni system below 1200 K. Met Trans 1986;17A: 1361.
[27] Chuang Y-Y, Chang YA. A thermodynamic analysis and calculation of the Fe-Ni-Cr phase diagram. Metall Trans A 1987;18A:733.
[28] Hsieh K-C, Chang YA. Thermochemical description of the ternary iron-nickel-sulfur system. Can Met Quarterly 1987;26:311.
[29] Chen S-W, Jan C-H, Lin J-C, Chang YA. Phase equilibria of the Al-Li binary system. Met Trans A 1989;20A:2247.
[30] Kattner UR, Lin J-C, Chang YA. Thermodynamic assessment and calculation of the Ti-Al system. Met Trans 1992;23A:2081.
[31] Murray J, Peruzzi A, Abriata JP. J Phase Equilibria (USA) 1992;13:277.
[32] Chen S-L, Chang YA. A thermodynamic analysis of the Al-Zn system and phase diagram calculation. CALPHAD 1993;17:113.
[33] Sundman B, Jansson B, Anderson J-O. CALPHAD 1985;9:153.
[34] Eriksson G, Hack K. Metall Trans B 1990;21B:1013.
[35] Thompson WT, Eriksson G, Bale CW, Pelton AD. Applications of F*A*C*T in high temperature materials chemistry. Electrochemical Society, Inc (USA) 1997:16–30.
[36] Dinsdale AT, Hodson SM, Barry TI, Taylor JR. Proc. 27th Annual Conference of Metallurgists, CIM, Montreal, 1988. Computations using MTDATA of metal-matte-slag-gas equilibria. 11, 59.
[37] Andersson J-O, Guillermet AF, Hillert M, Jasson B, Sundman B. Acta Metall 1986;34:437.
[38] Lukas HL, Weiss J, Kattner U, Henig E-Th. Manual of the computer programs BINGSS, TERGSS, QUAGSS, BINFKT, QUAFKT, AND PMLFKT, version 11, Jan 1988.
[39] Oates WA, Wenzl H. CALPHAD 1992;16:73.
[40] Oates WA, Wenzl H. CALPHAD 1993;17:35.
[41] Chen S-L, Kao CR, Chang YA. Intermetallics 1995;3:233.
[42] Zhang F, Huang W, Chang YA. CALPHAD 1997;21:337.
[43] Bragg WL, Williams EJ. Proc Roy Soc 1934;A145:699.
[44] Bragg WL, Williams EJ. Proc Roy Soc 1935;A151:540.
[45] Wagner C, Shottky W. Z Phys Chem 1930;B11:163.
[46] Chen S-L, Daniel S, Zhang F, Chang YA, Oates WA, Schmid-Fetzer R. On the calculation of multicomponent stable phase diagrams. J Phase Equilibria 2001;22:373–8.
[47] PANDAT software for multicomponent phase diagram calculation by computherm, LLC, 437 S. Yellowstone Dr., Madison, WI. 2000.
[48] Chen S-L, Chou K-C, Chang YA. On a new strategy of phase diagram calculation, 1. Basic principles. CALPHAD 1993;17:237.
[49] Chen S-L, Chou K-C, Chang YA. On a new strategy of phase diagram calculation, 2. Binary systems. CALPHAD 1993;17:287.
[50] Muggianu YM, Gambino M, Bros JP. J Chimie Physique 1975;72:83.
[51] Liang, H. Thermodynamic modeling and experimental investigation of the Al-Cu-Mg-Zn quaternary system. Ph.D. Thesis, University of Wisconsin, Madison, WI., 1998.
[52] Daniel S, Chang YA. unpublished work, University of Wisconsin, Madison, WI., 2001.
[53] Yan X-Y, Chang YA, Xie F-Y, Chen S-L, Zhang F, Daniel S. Calculated phase diagrams of aluminum alloys from binary Al-Cu to multicomponent commercial alloys. J Alloy Compounds 2001;320:151–60.
[54] PanAluminum—A thermodynamic database for a 14 component aluminum alloy system, 2001, CompuTherm, LLC, 437 S. Yellowstone Dr., Madison, WI.

[55] Yan X-Y, Chang YA, Yang Y, Xie F-Y, Chen S-L, Zhang F, Daniel S, He M-H. A thermodynamic approach for predicting the tendency of multicomponent metallic alloys for glass formation. Intermetallic 2001;9:535–8.
[56] Lin XH, Johnson WL. J Appl Phys 1995;78:6514.
[57] Kracek FC. J Phys Chem 1930;34:1588.
[58] Chang YA, Neumann JP, Mikula A, Goldberg D. INCRA Monograph VI. Phase diagrams and thermodynamic properties of ternary copper–metal systems. New York: The International Copper Research Association, Inc.; 1979.
[59] Chang YA, Neumann JP, Choudary UV. INCRA monograph VII. Phase diagrams and thermodynamic properties of ternary copper–sulfur–metal systems. New York: The International Copper Research Association, Inc.; 1979.
[60] Chang YA, Hsieh K-C. Phase diagrams of ternary copper-oxygen-metal systems. Metals Park, OH: ASM International; 1989 44073.
[61] Rhines F. Phase diagrams in metallurgy, their development and applications. New York: McGraw-Hill; 1951.
[62] WinPhad software for binary phase diagram calculation by CompuTherm, LLC, 437 S. Yellowstone Dr., Madison, WI. 53719, 1998.
[63] Zhang F. CompuTherm, LLC, 437 S. Yellowstone Dr., Madison, WI. Private communication, 2001.
[64] Ansara I, Dinsdale AT, Rand MH. Editors, COST 507: Thermochemical Database for Light Metals Alloys, European Communities, Luxembourg, ISBN 92-828-3902-8, 1998.
[65] Hillert M, Staffanson LI. Acta Chem Scand 1970;24:3618.
[66] Harvig H. Acta Chem Scand 1971;25:3199.
[67] Sundman B, Agren J. J Phys Chem Solids 1981;42:297.
[68] Dupin N, Ansara H. J Phase Equilibria 1993;14:451.
[69] Zhang F, Chen S-L, Chang YA, Oates WA. An improved approach for obtaining thermodynamic descriptions of intermetallic phases: application to the Cr-Ta System. Intermetallics 2001;9:1079–83.
[70] Zhang F, Chen SL, Chang YA, Kattner UR. A thermodynamic description of the Ti-Al system. Intermetallics 1997;5:471.
[71] Du Y, Clavagurea N. J Alloys and Comp 1996;237:20–32.
[72] Ansara I, Dupin N, Lukas HL, Sundman B. J Alloys and Comp 1997;247:20–30.
[73] Huang W, Chang YA. A thermodynamic analysis of the Ni-Al system. Intermetallics 1998;6:487–98 Corrigendum: Intermetallics, 1999, 7, 625-626.
[74] Chang YA, Chen S-L, Zhang F, Oates WA. Improving multicomponent phase diagram calculations. In: Turch PEA, Gonis A, Shull RD, editors. CALPHAD and Alloy Thermodynamics. Warrendale, PA: TMS; 2002. p. 53–60.
[75] Zhang F, Chang YA, Du Y, Chen S-L, Oates WA. Modeling of the fcc phases using the cluster-site approximation in the Ni-Al system. Acta Mater 2003;51:207–16.
[76] Oates WA, Wenzl H, Mohri T. CALPHAD 1996;20:37.
[77] Redlich O, Kister A. Ind Eng Chem 1948;40:345.
[78] de Fontaine D. Solid State Physics 1994;47:33–176.
[79] Oates WA, Wenzl H. The cluster/site approximation for multicomponent solutions-a practical alternative to the cluster variation method. Scr Mater 1989;35:623.
[80] Oates WA, Zhang F, Chen S-L, Chang YA. An improved cluster/site approximation for the entropy of mixing in multicomponent solid solutions. Phys Rev B 1999;59B:11221–5.
[81] Yang CN. A generalization of the quasi-chemical method in the statistical theory of superlattices. J Chem Phys 1945;13:66.
[82] Yang CN, Li YY. Generalized theory of the quasi-chemical method in the statistical theory of superlattices. Chinese J Phys 1947;7:59.
[83] Li YY. Quasi-chemical theory of order for the copper gold system. J Chem Phys 1949;17:447.
[84] Li YY. Quasi-chemical method in the statistical theory of regular mixtures. Phys Rev 1949;76:972.
[85] Kikuchi R. Phys Rev 1951;81:988.

[86] Lee J. New Monte Carlo algorithm: entropic sampling. Phys Rev Lett 1993;71:211.
[87] Ferreira LG, Wolverton G, Zunger A. Valuating and improving the cluster variation method entropy functional for Ising alloys. J Chem Phys 1998;108:2912.
[88] Ferreira LG, Mbaye AA, Zunger A. Effect of chemical and elastic interactions on the phase diagrams of isostructural solids. Phys Rev 1987;B35:6475.
[89] Zhang J, Oates WA, Zhang F, Chen S-L, Chou K-C, Chang YA. Cluster/site approximation of the ordering phase diagram for Cd-Mg alloys. Intermetallics 2001;9:5–8.
[90] Frantz C, Gantois M. J App Crystallog 1971;4:387.
[91] Asta M, McCormack R, de Fontaine D. Phys Rev B 1993;48:748.
[92] Zhang F, Oates WA, Chen S-L, Chang YA. Cluster-site approximation (CSA) calculation of phase diagrams. In: McNallan M, Opila E, editors. High Temp.erature Corrosion and Materials Chemistry III. The Electrochemical Society, Pennington, NJ; 2001. p. 241–52 12.
[93] Sigli C, Sanchez JM. Acta Mater 1985;33:1097.
[94] Pasturel A, Colinet C, Paxton AT, van Schilfgaaarde M. J Phys Condens Matter 1992;4:945.
[95] PanEngine is the calculation engine from PANDAT, a Dynamically Linked Library (DLL) that can be used to create custom software applications, 2001, CompuTherm, LLC, 437 S. Yellowstone Dr., Madison, WI.
[96] Chang YA, Yan X-Y, Daniel SL, Xie F-Y, Chen S-L, Zhang F. PANDA and PanEngine—their applications in multicomponent phase diagram calculation and microstructure prediction. In: Zhao J-C, Fahrmann M, Pollock TM, editors. Materials design approaches and experiences. Warrendale, PA: TMS; 2001. p. 85–96.
[97] Xie F-Y, Kraft T, Zuo Y, Moon C-H, Chang YA. Acta Mater 1999;47:489–500.
[98] Xie F-Y. Ph.D. Thesis, University of Wisconsin–Madison, 1999.
[99] Liang H, Kraft T, Chang YA. Importance of reliable phase equilibria in studying microsegregation in alloys: Al-Cu-Mg. Mater Sci Engin 2000;A292:96–103.
[100] Xie F-Y, Kraft T, Chu M, Chang YA. Microstructure and microsegregation in a directionally solidified quaternary Al-rich Al-Cu-Mg-Zn Alloy. In: Anjier JL, editor. Light Metals 2001. Warrendale, PA: TMS; 2001. p. 1085–90.
[101] Yan XY, Ding L, Chen S-L, Xie F-Y, Chu M, Chang YA. Predicting microstructure and microsegregation in multicomponent aluminum alloys. In: Anjier JL, editor. Light metals 2001. Warrendale, PA: TMS; 2001. p. 1091–7.
[102] Yan X-Y, Xie F-Y, Chu M, Chang YA. Microsegregation in Al-4.5Cu wt pct Alloy: Experimental investigation and numerical modeling. Mater Sci Engin 2001;A302:268–74.
[103] Xie F-Y, Yan X-Y, Ding L, Zhang F, Chen S-L, Chu M, Chang YA. A study of microstructure and microsegregation on aluminium 7050 alloys. Mater Sci Engin 2003;A:in press.
[104] Bellen P, Hari Kumar KC, Wollants P. Z Metallkd 1996;87:972.